ACS NANO

www.acsnano.org

ARTICLE

Bionic Enzyme-Assisted Ion-Selective Amperometric Biosensor Based on 3D Porous Conductive Matrix for Point-of-Care Nitrite Testing

Han Wang,*,# Xueqi Wang,# and Jing Cheng

Cite This: *ACS Nano* 2022, 16, 14849–14859

Read Online

ACCESS | Metrics & More | Article Recommendations | Supporting Information

ABSTRACT: Nitrite plays a critical role in a variety of physiological processes and maintaining the nitrite level in an appropriate range is vital to keep healthy. Current nitrite analysis methods lack sensitivity and require tedious operations, which could not meet the need of point-of-care (POC) nitrite detection in precision medicine. Here we present a cyanocobalamin (VB_{12}) bionic enzyme-assisted ion-selective amperometric biosensor based on 3D porous conductive matrix (PCM), which can facilitate rapid and accurate POC nitrite monitoring in complex biofluids. The experimental findings quantitatively demonstrate that the biosensor has a sensitivity of 64.08 $\mu A/(mM \cdot cm^2)$, a wide linear range of 0.025−45 mM, and low limit of detection of 1 nM. Moreover, the developed VB_{12}/BSA-PCM biosensor shows outstanding stability after 21 days with 2% decline in current signal, and high repeatability between batches with RSD of only 1.29%. Real salivary nitrite detection has been evaluated, and the results match well with the commercial nitrite analyzer. Thus, the bionic enzyme-assisted ion-selective amperometric biosensor proposed herein has potential utility as an affordable tool for POC detection and home-based healthcare.

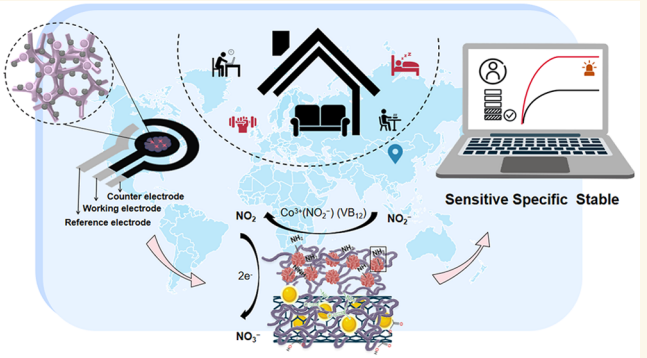

KEYWORDS: *amperometric biosensor, electrochemical testing, bionic enzyme, ion-selective electrode, saliva nitrite detection, POC testing*

Stomach cancer is the fourth leading cause of cancer deaths worldwide, where the rate of median survival is less than 12 months for the advanced stage.[1] One of the biological causes of stomach cancer is the chronic elevation of blood nitrite level caused by abnormal metabolism, which gradually leads to the accumulation of endogenous N-nitroso compounds.[2] Besides, a lasting high nitrite level in the human body can also cause other severe diseases including anemia, lactic acidosis,[3] spontaneous abortion, and blue baby syndrome.[4] However, for nitrite, less is not always better. A moderate level of nitrite is not only necessary to prevent and treat fatty liver,[5] but also significant to regulate vascular functions.[6] Thus, maintaining blood nitrite level at an appropriate range is vital to keep healthy. However, nitrite concentration fluctuates greatly at the early stage of a metabolic disorder without obvious symptoms. Therefore, regular detection of nitrite levels in the body to distinguish an abnormal metabolism is important for the diagnosis, treatment, and prognosis of a variety of diseases especially stomach cancer.

Among all kinds of body fluids, saliva has been considered promising for accurate, fast, and noninvasive detection of nitrite. For one thing, saliva, as the body fluid with the highest nitrite concentration and strongest correlation with blood nitrite,[7] can be utilized to effectively reflect the metabolism of nitrite in the whole body. For another, saliva can be examined conveniently in a noninvasive manner with the lowest discomfort and shortest sampling time, making routine salivary nitrite detection feasible. Therefore, saliva nitrite analysis is a potential approach for noninvasive nitrite detection to realize early disease diagnosis and long-term health management. So far, various methods based on spectrophotometry,[8] chem-

Received: June 11, 2022
Accepted: September 8, 2022
Published: September 13, 2022

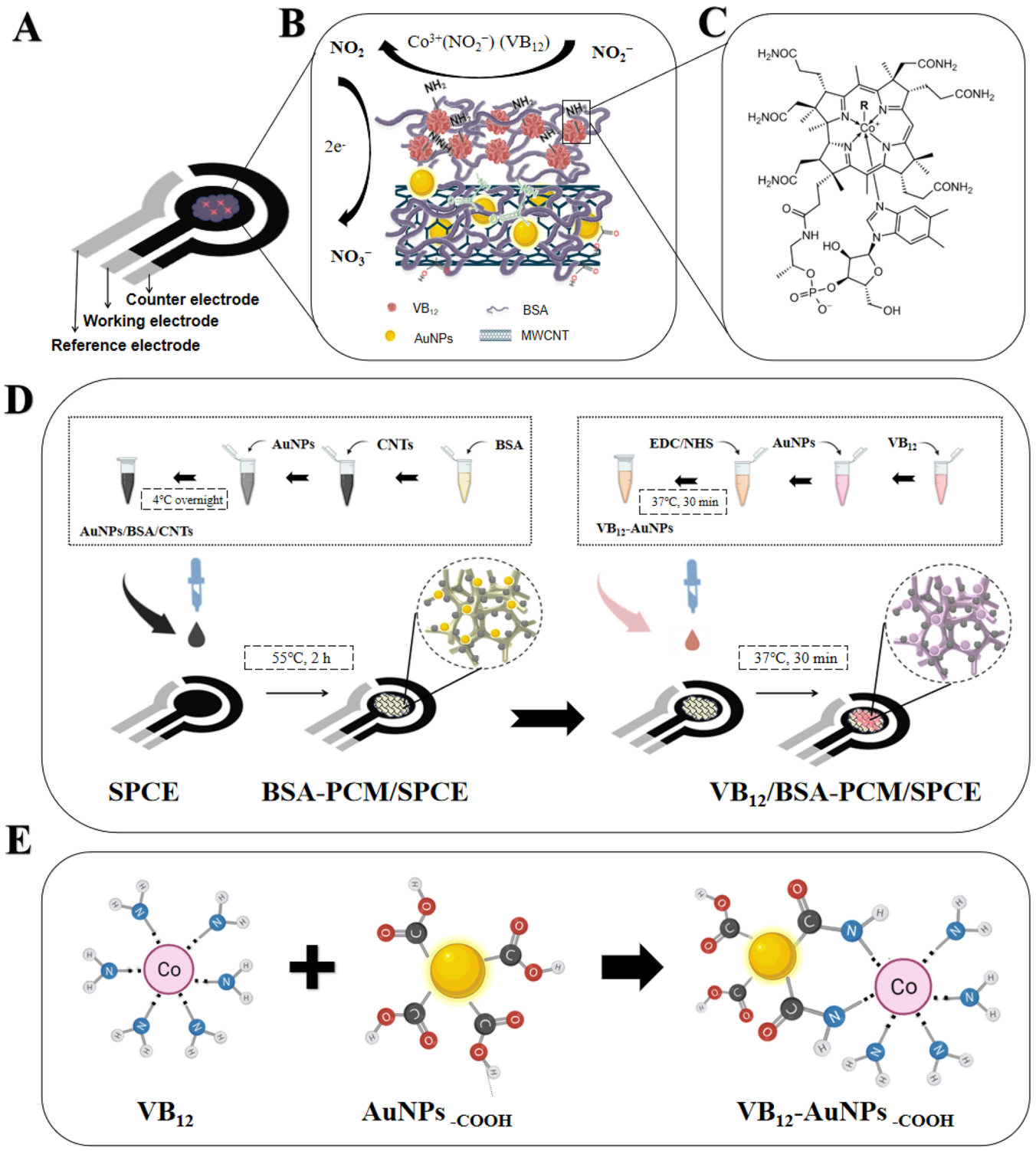

Figure 1. Schematic illustration of the design and construction of VB_{12}/BSA-PCM electrochemical biosensor for nitrite detection. (A) The screen-printed carbon electrode is composed of a three-electrode system, where the working electrode is modified by AuNPs/BSA/CNTs solution and VB_{12} solution in sequence. (B) Configuration of the 3D VB_{12}/BSA-PCM sensing interface on the working electrode. (C) Structural formula of VB_{12}. (D) Schematic illustration of detailed fabrication processes of the VB_{12}/BSA-PCM electrochemical biosensor. (E) Schematic diagram of covalent combination between VB_{12} and carboxyl modified AuNPs.

iluminescence,[9] high-performance liquid chromatography (HPLC),[10,11] and so forth have been implemented to analyze salivary nitrite. Although these techniques can test nitrite with high sensitivity, they suffer from complex sample pretreatment and long processing time, and require cumbersome instruments. Thus, convenient and rapid detection methods with excellent sensitivity, high specificity, and low-cost for salivary nitrite detection are in urgent need.

Point-of-care testing (POCT), taking advantage of their portability, short processing time, and small sample consumption, shows promising applications in community and home-based disease management and has the potential to

https://doi.org/10.1021/acsnano.2c05752
ACS Nano 2022, 16, 14849−14859

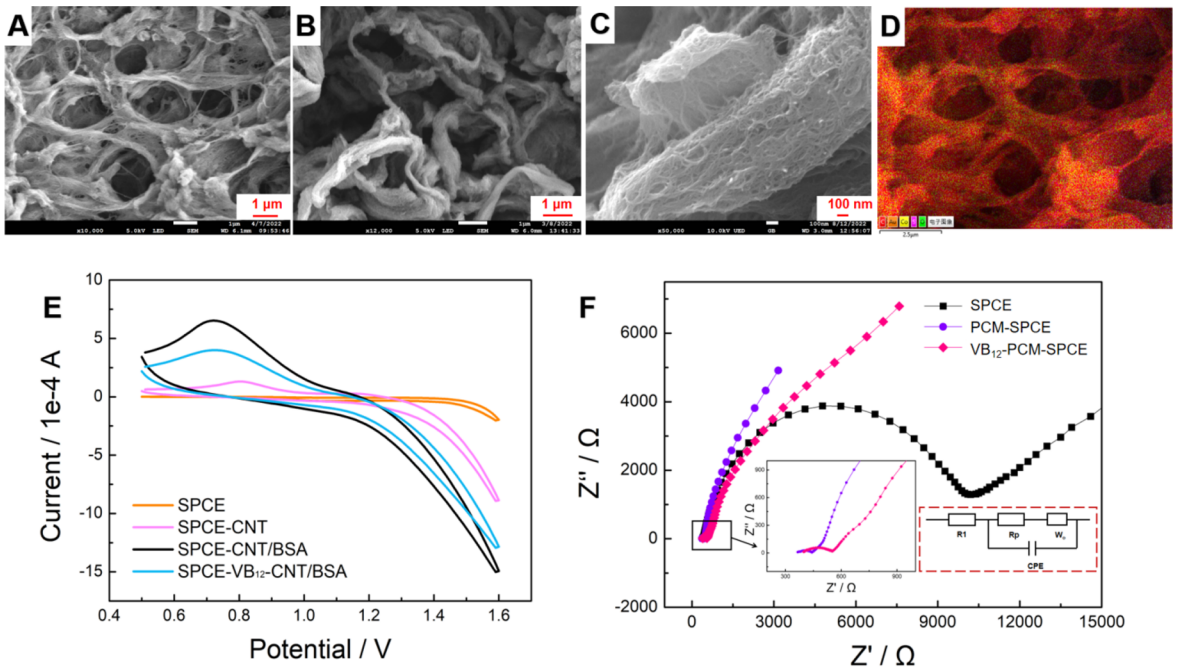

Figure 2. Property characterization of VB_{12}/BSA-PCM biosensor. SEM images of the PCM surface at (A) 10,000 times magnification, (B) 12,000 times magnification, and (C) 50,000 times magnification. (D) EDS image of the VB_{12}/BSA-PCM at 10,000 times magnification. (E) Cyclic voltammetry response of the bare SPCE, SPCE-CNTs, SPCE-CNTs/BSA, and SPCE-VB_{12}−CNTs/BSA electrode in 2 mM $NaNO_2$ solution at the scanning rate of 100 mV/s. (F) Nyquist plots of EIS results of the bare SPCE, SPCE-CNTs/BSA, and SPCE-VB_{12}-CNTs/BSA electrodes in 1 mM $[Fe(CN)_6]^{3-/4-}$ containing 0.1 M KCl solution. The inset shows enlarged view of the EIS result of SPCE-CNTs/BSA and SPCE-VB_{12}-CNTs/BSA electrodes, while the equivalent circuit is shown in the dashed box.

achieve decentralized medicine.[12] Among all POCT methods, electrochemical methods with high sensitivity, rapid response, and low cost have attracted wide attention. Nitrite, as an electrocatalytic active substance prone to redox, is particularly suitable for electrochemical detection. Therefore, an electrochemical biosensor provides a promising method for convenient, rapid, and accurate point-of care nitrite detection.

So far two types of electrochemical biosensors have been developed for nitrite detection, amperometric biosensors based on conductive nanomaterials, and potentiometric biosensors based on ion-selective membranes. Amperometric biosensors utilize different kinds of electroactive materials including MoS_2 microsphere,[13] Au nanoparticles(AuNPs)/graphene oxide,[14] AuNPs/polyaniline/SnO_2 nanocomposite,[15] and so on to improve the sensitivity of nitrite detection. However, these biosensors suffer from low selectivity and inaccuracy. To overcome this problem, potentiometric ion-selective biosensors based on cobalt phthalocyanine,[16] lipophilic Co^{2+}, *tert*-butylsalophen ionophore,[17] Schiff base-derived Co^{3+} complex,[18] and so on, show high selectivity to nitrite since cobalt ions can specifically recognize and strongly interact with nitrite. However, these potentiometric biosensors require long response time and are only effective in acidic conditions, making pretreatment of the saliva sample indispensable. Therefore, developing an electrochemical biosensor with high sensitivity, high selectivity, short response time, and simple sample processing for point-of-care nitrite monitoring is of great importance.

In this work, we present a bionic enzyme-assisted ion-selective amperometric biosensor for point-of-care salivary nitrite detection. While cyanocobalamin (VB_{12}) bionic enzyme forms an ion-selective layer to specially capture and oxidize nitrite, bovine serum albumin (BSA)-based PCM constructs the solid contact layer to immobilize bionic enzyme and prompts the transfer of electrons generated by redox on the ion-selective layer, simultaneously improving the sensitivity and selectivity of the biosensor. On the one hand, PCM is formed through carbon nanotubes (CNTs) modification and BSA cross-linking,[19,20] resulting in conductive 3D porous structures that greatly improve the surface-to-volume ratio. This increases the immobilization density of VB_{12} bionic enzymes and enlarges the area in contact with saliva samples, endowing the biosensor outstanding electron conductivity, high sensitivity, and good stability. On the other hand, VB_{12} bionic enzyme modification is based on covalent binding, which enhances the stability of the ion-selective layer and generates a stronger field ligand between PCM and nitrite, improving the selectivity of the nitrite biosensor in complex biological fluids. To assess the characteristics of this POC nitrite biosensor, we performed electrochemical tests with standard nitrite solutions and real saliva samples to evaluate its stability, sensitivity, and selectivity. We envision that the presented biosensor can be a promising tool for POCT and home-based healthcare in the future.

RESULTS/DISCUSSION

Property Characterization of the VB_{12}/BSA-PCM Biosensor. The developed electrochemical biosensor is based on the proposed 3D VB_{12}/BSA-PCM electrode interface. Figure 1(A) shows the configuration of the developed 3D VB_{12}/BSA-PCM electrochemical biosensor. The working electrode in Figure 1(B,C) consists of the BSA-PCM based solid contact layer and VB_{12} bionic enzyme-based ion-selective layer. On the one hand, BSA-PCM greatly increases the immobilization density of the CNTs and VB_{12} bionic enzyme, endowing the biosensor high electron

https://doi.org/10.1021/acsnano.2c05752
ACS Nano 2022, 16, 14849−14859

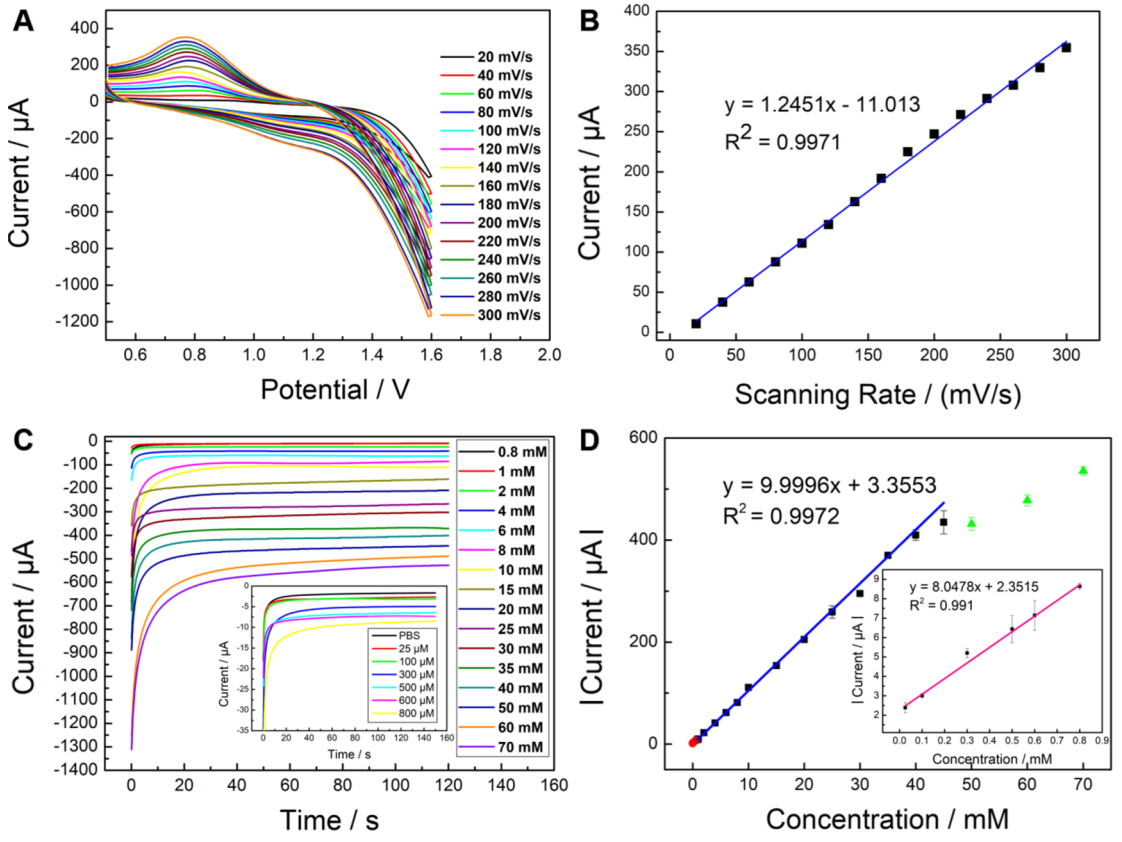

Figure 3. Performance characterization of the VB_{12}/BSA-PCM biosensor. (A) Cyclic voltammograms of 2 mM $NaNO_2$ catalyzed by VB_{12}-BSA/PCM electrode at scanning rates of 20−300 mV/s with an interval of 20 mV/s. (B) Plot of peak oxidation currents versus scanning rates. The peak oxidation current increased as the scanning rate increased in a linear manner. (C) Amperometric *i*−*t* curves of the VB_{12}-BSA/PCM electrode in different concentrations of nitrite. (D) The linear curve fitting of the absolute values of steady-state currents and nitrite concentrations ranging from 0.8 mM to 45 mM. The inset shows the linear curve fitting with nitrite concentrations ranging from 0.025 mM to 0.8 mM.

conductivity and good stability. On the other hand, VB_{12} bionic enzyme coating generates a stronger field ligand between PCM and nitrite, improving the selectivity and specificity of the nitrite biosensor in complex biological fluids. The BSA-PCM electrochemical biosensor was successfully fabricated and modified with VB_{12} (seen from Figure 1(D), methods), and after combining the advantages of BSA-PCM and VB_{12} bionic enzyme, an amperometric ion-selective electrode with excellent selectivity and high sensitivity was developed. What is more, the whole interface does not involve any organic enzymes or other volatile substances, and VB_{12} bionic enzyme is immobilized on the surface of BSA-PCM by covalent bonds (Figure 1(E)), endowing the sensor excellent stability and a long working life.

Figure 2(A−D) and Figure S1 show the surface microstructure of the working electrode of the screen-printed carbon electrode (SPCE) before and after VB_{12}/BSA-PCM modification. The rough surface of the bare carbon electrode without modification, as can be seen in Figure S1(A,B), is conducive to the stable attachment of the PCM layer. After BSA-PCM immobilization by the drop casting method, the surface of the SPCE was covered by a porous, sponge-like protein skeleton, as seen from the SEM image in Figure 2(A). To be specific, the BSA-PCM had apertures of about 1 μm, which uniformly distributed on the surface of the skeleton. When the magnification of SEM increases further, the organic layer on the surface of BSA-PCM can be clearly seen in Figure 2(B,C), which preliminarily verified the successful modification of the ion-selective membrane on the conductive porous skeleton. The ion-selective membrane is immobilized by the carboxyl modified AuNPs, which has a regular shape and uniform size about 20 nm, as seen in Figure S1(C). Further, the EDS and TEM images shown in Figure 2(D) and Figure S1(D−F) demonstrate the introduction of cobalt ions and AuNPs, supporting the successful immobilization of VB_{12} bionic enzymes on the upper surface of BSA-PCM. Additionally, the surface profile of the electrodes before and after modification was measured by an atomic profiler and the result is shown in Figure S1(G), where the developed VB_{12}/BSA-PCM layer has a thickness of about 20 μm. On the one hand, the developed staggered 3D porous skeleton structure greatly increases the adhesion surface area of VB_{12} and promotes the rapid transfer of electrons, which improves the sensitivity of the sensor while ensuring the selectivity. On the other hand, it effectively protects the conductive layer that assists the electron transfer, avoiding the damage of the conductive interface in complex biofluids as much as possible.

The electrochemical properties of the bare SPCE, SPCE-CNTs, SPCE-CNTs/BSA, and SPCE-VB_{12}-CNTs/BSA were recorded by cyclic voltammetry in 2 mM $NaNO_2$ solution. As shown in Figure 2(E), the SPCE-CNTs/BSA electrode exhibited excellent peak current response, suggesting our developed BSA-PCM skeleton had outstanding electroconductibility, and allowed electrons to transfer with low

https://doi.org/10.1021/acsnano.2c05752
ACS Nano 2022, 16, 14849−14859

Table 1. Comparison of the Analytical Performance of the VB_{12}-BSA/PCM Biosensor in This Work with Other Detection Methods, Especially with Those of Electrochemical Sensors

method	specificity	linear range/mM	LOD/μM	working condition	ref
		Chromatography			
VIM-EDMA column	Medium	0.27−54	0.001	Neutral	22
		Colorimetry			
P−N (1,2-diaminoanthraquinone) fluorescent probe	Excellent	0−0.016	0.054	Neutral	23
CQD/3-Aph fluorescent probe	Excellent	0.0025−0.1	0.001	Acidic	24
		Electrochemistry			
ZIF-8@ZIF-67/Au NPs/GCE	Poor	0.00064−22	0.002	Neutral	25
AuNPs/GO-SH	Poor	0.005−1.0	0.25	Neutral	26
(HOOC-MWCNTs) /GCE	Poor	0.1−0.7	0.565	Neutral	27
GO-PANI-AuNPs-GEC	Poor	0.24−2.58	0.17	pH = 6.0	13
Cobalt(II)*tert*-butyl salophen ionophore	Excellent	0.01−10	1.0	pH = 3.1	16
EAB	Excellent	0.006−2.1	0.28	pH= 7.6−8.6	17
Hb/Au/GACS/GC	Medium	0.00005−1	0.01	Neutral	28
Hb/poly(nBA)-rGO/SPE	Medium	0.001−0.1	0.65	Neutral	29
L-Arginine/Co_3O_4/FTO	Medium	0.01- 16	0.00195	Neutral	30
VB_{12}-BSA/PCM	**Excellent**	**0.025−45**	**0.001**	**pH = 5.0−9.0**	**This work**

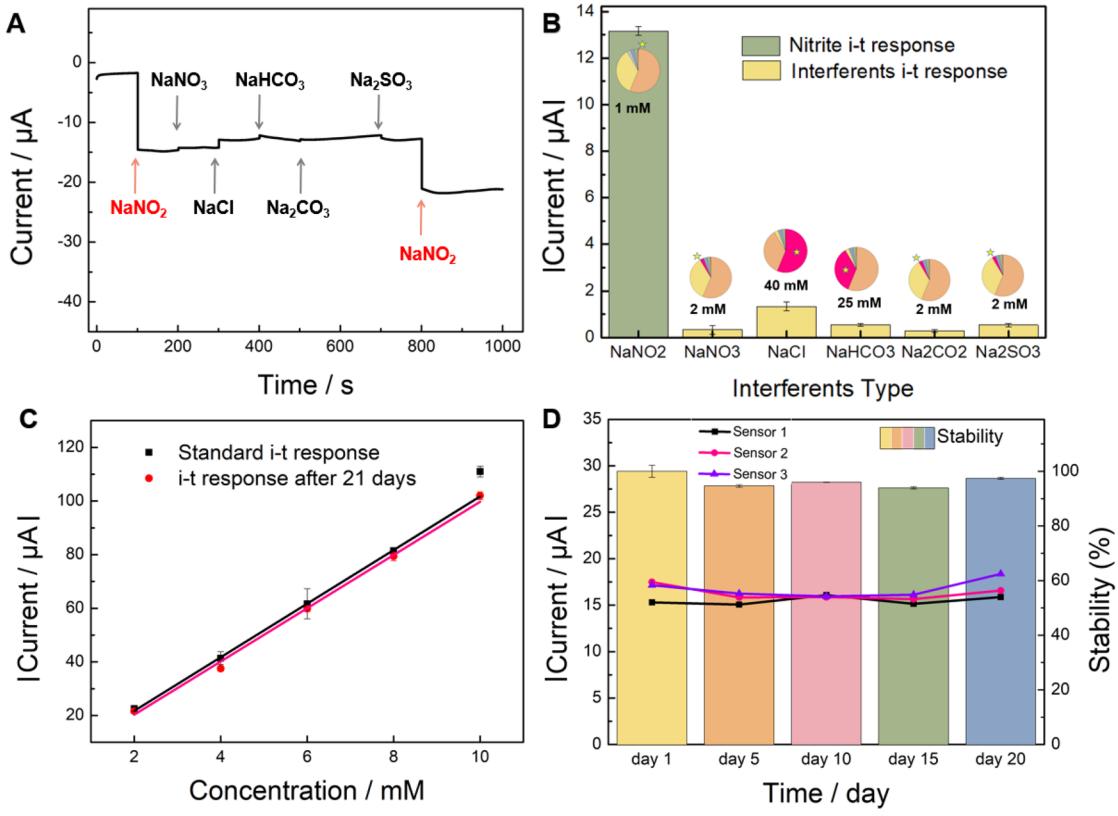

Figure 4. Selectivity and stability characterization of VB_{12}-BSA/PCM biosensor. (A) Selectivity test of VB_{12}-BSA/PCM biosensor by adding NaCl at 40 mM, $NaHCO_3$ at 25 mM. (B) The bar graph of the absolute values of response currents of VB12-BSA/PCM biosensor of nitrite and interferents. The pie chart mainly shows the proportion of different interferents in the solution, and the deep pink part of the pie chart shows the concentration proportion of the corresponding substance. (C) Stability test results of the VB_{12}-BSA/PCM biosensor in nitrite solution before (black, N = 3) and after (red, N = 3) storage in a refrigerator at 4 °C for 21 days. (D) Stability of the VB_{12}-BSA/PCM biosensor in nitrite detection for the duration of 20 days. Bar graph shows the stability of the biosensors, and the line chart inset shows the current response of three biosensors selected randomly. The biosensors were retrieved every 5 days from 4 °C refrigerator, and the performance was investigated by amperometric i−t measurement using the nitrite solution at the concentration of 2 mM. Error bars are the standard error of the mean (N = 3).

hindrance. Upon subsequent immobilization of VB_{12} bionic enzyme, a semi-insulating ion-selective layer was formed and blocked the charge transfer between the electrode and the substance that could not bond to the membrane, so that a decrease in peak current was observed for SPCE-VB_{12}-CNTs/BSA. These results demonstrated outstanding electrocatalytic performance of the SPCE-VB_{12}-CNTs/BSA electrode for nitrite detection. Further, the interfacial properties of bare SPCE, SPCE-CNTs/BSA, and SPCE-VB12-CNTs/BSA were compared by conducting EIS tests. As seen from Figure 2(F),

https://doi.org/10.1021/acsnano.2c05752
ACS Nano 2022, 16, 14849−14859

the Nyquist diagram comprises a semicircle in the range of high frequencies and a linear part in the range of low frequencies, representing an electron transfer-limited process and diffusion-limited process, respectively. Then, the Randles model is used to calculate the kinetics parameters of electron transfer, which includes solution resistance (R_1) in series with a parallel combination of constant phase element (CPE) and electron transfer resistance (R_p) together with Warburg resistance (R_w). The electron transfer resistance decreased significantly from bare SPCE (9044 Ω) to SPCE-CNTs/BSA (86 Ω), demonstrating that the CNTs/BSA modification endows the SPCE excellent conductivity. R_p of SPCE-VB_{12}−CNTs/BSA (143.9 Ω) increased slightly due to the composite of semi-insulating ion-selective layer, consistent with the results obtained by CV measurements.[21]

For optimization of the working potential, the response currents of nitrite were recorded under both low and high nitrite concentration. The peak response current increased gradually as the working potential increased from 0.4 to 1.0 V and then decreased obviously when the potential was larger than 1.0 V (Figure S2). Therefore, the optimal working potential was determined to be 1.0 V for the following experiments.

Figure 3 panels A and B demonstrate the cyclic voltammograms of the VB_{12}-BSA/PCM biosensor under different scanning rates. The oxidation current increased as the scanning rate increased from 20 to 300 mV/s with 20 mV/s intervals (Figure 3(A)). In Figure 3(B), the peak oxidation current of cyclic voltammetry curves increased in a linear manner (R^2 > 0.997) as the scanning rate increased, which fits well with the Randled-Sevcik equation:

$$I_P = \frac{n^2F^2}{4RT}\nu A\Gamma^* \quad (1)$$

In eq 1, I_P is the peak current (A) in cyclic voltammograms, n represents the number of electrons transferred in the redox event, A stands for the electrochemical active area (cm^2) of the electrode, ν stands for the scanning rate (V/s), F represents Faraday constant, and Γ^*represents the specific area (mol/cm^2) of the reactants attached to the electrode surface. It is evident that the catalytic oxidation reaction of nitrite by VB_{12}-BSA/PCM electrode was surface adsorption controlled. To be specific, nitrite was first chelated with cobalt ion in VB_{12} and adsorbed on the surface of ion-selective layer, and then redox reaction was started to carry out electron transfer.

The amperometric i−t curves of different concentrations of nitrite solutions are presented in Figure 3(C,D). Figure 3(D) is the linear relationship between the absolute value of the current signal and the nitrite concentration. The linear range is divided into two sections, where the corresponding linear equations are $I(\mu A) = 9.9996C_{nitrite}$ (mM) + 3.3533, R^2 > 0.997, for nitrite concentrations of 0.025−0.8 mM, and $I(\mu A) = 8.0478C_{nitrite}$ (mM) + 2.351, R^2 = 0.991, for nitrite concentrations of 0.8−45 mM, respectively. According to the measured results, the LOD of the biosensor was calculated to be 1 nM and the sensitivity reached up to 64.08 μA/(mM·cm^2), which outperformed most of the previously reported nitrite electrochemical biosensors (Table 1) and could meet the clinical requirement for salivary nitrite detection.

To evaluate the selectivity of the fabricated VB_{12}-BSA/PCM biosensor, amperometric response was measured at the applied potential of 1.0 V by introducing nitrite and other interferents including nitrate, chloride, carbonate, bicarbonate, and sulfite. Figure 4 panels A and B show that the current response of the VB_{12}-BSA/PCM biosensor to nitrite is nearly 20 times higher than that of the interferents under the highest concentration level in healthy human saliva. The exhibited negligible effect of interferents of the biosensor indicated that the VB_{12}-BSA/PCM biosensor was feasible for specific detection of nitrite in the presence of other ions and biomolecules in saliva, demonstrating its potential in practical application for accurate and specific salivary nitrite detection.

In addition, the stability is of great significance to evaluate the performance of the developed biosensor. The morphological properties of the porous, sponge-like VB_{12}-BSA/PCM biosensor remains uniform after testing, 3 months storage, and testing following 3 months storage, seen from Figure S3(A−C). As shown in Figure S4(A), the CV responses of the VB_{12}-BSA/PCM biosensor before and after the durability experiment for 3 months are similar, and the peak currents almost coincide, ensuring the stability of the interfacial properties. Additionally, the selectivity of the biosensor after 3 months of storage is still excellent, and the current variation caused by interferents at physiological concentrations is negligible (see Figure S4(B)). What is more, as seen in Figure 4(C,D) and Figure S4(C,D), after 21 days of storage in a 4 °C refrigerator, the performance of the 3D VB_{12}-BSA/PCM electrochemical biosensor remained largely unchanged. After 21 days of storage, the absolute values of peak oxidation currents at the same concentration of nitrite, remained at least 98% compared to those before storage. The linear fitting curves of the peak oxidation currents before and after storage almost overlapped, both at low (Figure S4(C)) and high (Figure 4(C)) concentrations, suggesting excellent stability and a long working time of the VB_{12}-BSA/PCM biosensor.

Additionally, repeatability is also an important indicator for evaluating sensor performance. Five fabricated VB_{12}-BSA/PCM biosensors were randomly selected and measured when adding 10 mM nitrite in PBS. It can be seen from Figure S5(A) that the relative standard deviation (RSD) between the electrodes was only 1.29%, indicating that the difference between biosensor batches is negligible, which makes mass production of this type of biosensors promising. Besides, we took the damage of pungent liquid to the surface of the VB_{12}-BSA/PCM biosensor during eating into consideration. To assess the antijamming capability of the developed biosensor, milk, Sprite, ketchup, brine, acetic acid, and alcohol were adopted to represent common drinks, extremely salty and acid environments, and organic liquid environments, respectively. As seen from Figure S5(B), the difference of response currents before and after soaking the sensors in common drinks was within 7%, and in extreme pungent liquid was less than 12%, indicating that diet and an interfering environment did not cause significant damage to VB_{12}-BSA/PCM biosensors. What is more, Figure S6 shows overlapped i−t response in nitrite solutions under different pH values, meaning our VB_{12}-BSA/PCM biosensor is compatible with samples at different pH levels. Thus, biofluids can be detected directly without pH adjustment or sample purification. The results further proved that the developed VB_{12}-BSA/PCM biosensor could be a universal tool for rapid, accurate, robust point-of-care salivary nitrite detection without complex sample preprocessing steps.

Overall, our developed VB_{12}-BSA/PCM biosensor shows outstanding performance in sensitivity, selectivity, stability, repeatability, and has the potential to be applied without

https://doi.org/10.1021/acsnano.2c05752
ACS Nano 2022, 16, 14849−14859

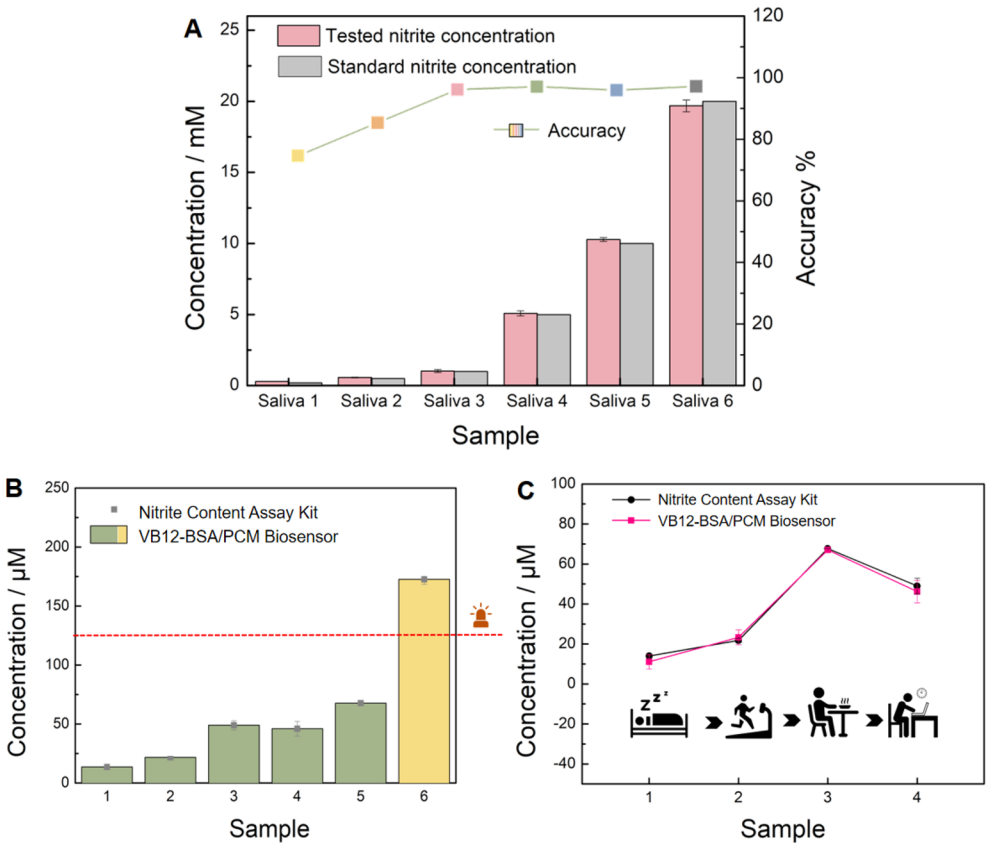

Figure 5. Practicability evaluation of the VB_{12}/BSA-PCM biosensor. (A) Determination of nitrite concentration in artificial saliva samples and in standard solution with the VB_{12}-BSA/PCM biosensor (N = 3). The inset line chart shows the accuracy of our developed VB_{12}-BSA/PCM biosensor in artificial saliva samples. (B) Determination of nitrite content in real saliva samples collected from human volunteers in multiple activity states. The red line marks the boundary between normal and abnormal nitrite concentrations. The green bars and the yellow bar indicate the nitrite concentrations below and exceeding the threshold, respectively. (C) Determination of nitrite content in real saliva samples collected from healthy human volunteers after different activities including sleeping, exercising, eating, and working with our biosensor and the commercial nitrite kit (N = 3).

complex sample preprocessing steps. Compared to the previously reported nitrite sensors (Table 1), our work is a step forward in building 3D porous amperometric ion-selective biosensors due to the PCM with larger contact area for the immobilization of CNTs, and VB_{12} bionic enzyme, which is helpful in improving its sensitivity and selectivity. To be specific, this work demonstrated a 3D porous amperometric ion-selective nitrite biosensor with low LOD and wide linear range, which has potential utility in salivary nitrite detection of clinical samples and nitrite metabolism disorder diagnosis.

Practicability Evaluation of the VB_{12}/BSA-PCM Biosensor. To evaluate the feasibility of the VB_{12}-BSA/PCM biosensor in practical applications, we first evaluated the biosensor with artificial saliva samples spiked with $NaNO_2$ solution, and then assessed its performance in sensing nitrite from real saliva samples of healthy human volunteers. The current response of the developed sensor was examined using artificial saliva samples spiked with standard nitrite solution to a final concentrations of 0.2, 0.5, 1, 5, 10, and 20 mM. The response current was converted to nitrite concentration using linear curve fitting of the VB_{12}-BSA/PCM biosensor, and the relative error values were negligible, as shown in Figure 5(A) and Table S1. The results demonstrated that the accuracy of the 3D PCM biosensor can satisfy the needs for nitrite detection in saliva samples.

For real saliva sample test using the developed VB_{12}-BSA/PCM biosensor, both disease warning and health management scenarios were simulated and tested. First, six saliva samples from human volunteers in any activity state were collected and analyzed by both the VB_{12}-BSA/PCM biosensor and a commercial nitrite assay kit. We set 125 μM salivary nitrite as the threshold of diseased states[31] and would give an alarm to the samples that exceeded the threshold, as shown in Figure 5(B). The nitrite concentration detected by our VB_{12}-BSA/PCM biosensor was highly consistent with the results of the commercial nitrite kit. Both the biosensor and the nitrite kit ring alarm for the abnormal nitrite concentration of volunteer 6, implying the imbalance of nitrite metabolism of the volunteer. Short-term overshoot of salivary nitrite may be caused by oral ulcer, frequent long vigils, or an inordinate daily schedule, while a long-term abnormality requires attention for the possibility of a series of sever diseases. Based on the above results, the accuracy of our developed VB_{12}-BSA/PCM biosensor for salivary nitrite detection was verified, and the capability of early detection of abnormal nitrite levels of the biosensor was proven to be effective.

Next, saliva samples from one healthy volunteer were collected and analyzed under different activities, including sleeping, exercising, eating, and working. As can be seen from Figure 5(C), compared to a commercial nitrite assay kit, our VB_{12}-BSA/PCM biosensor showed excellent sensitivity and

https://doi.org/10.1021/acsnano.2c05752
ACS Nano 2022, 16, 14849−14859

can effectively visualize the nitrite fluctuations during different metabolism states. Besides, since the VB_{12}-BSA/PCM biosensor possesses excellent selectivity and antijamming ability, sample processing can be simplified or omissible, retaining the content of salivary nitrite to the maximum extent during sample processing and ensuring that the detection result is accurate and reliable. What is more, it takes less than 7 min for unskilled personnel to complete the salivary nitrite detection using our portable VB_{12}-BSA/PCM biosensor, while it takes at least 40 min to accurately detect salivary nitrite using a commercial nitrite kit with the help of a cumbersome microplate reader and frequent standardization. Thus, the VB_{12}-BSA/PCM biosensor for nitrite detection was nearly 6 times faster than the commercial kit, which is extremely time-saving and use-friendly, making home-based routine salivary nitrite monitoring feasible and promising.

CONCLUSIONS

In this work, we have successfully developed a portable, robust, and low-cost ion-selective electrochemical biosensor for point-of-care testing with high sensitivity, high selectivity, high stability, wide linear range, and short response time. The developed VB_{12}-BSA/PCM electrochemical biosensor, as a special kind of bionic enzyme-assisted ion-selective amperometric biosensor, demonstrates high sensitivity and selectivity, making accurate, specific, and rapid point-of-care nitrite detection in complex biofluids feasible and promising.

To be specific, the VB_{12} bionic enzyme can generate a strong field ligand to capture nitrite in complex biofluids, and then Co^{3+} bound to nitrite can induce redox reactions rapidly under an appropriate voltage. The process does not involve any organic enzymes or other volatile substances, and therefore the biosensor is not affected by temperature, pH, or other interfering conditions, endowing the sensor excellent selectivity, high stability, and long working life. Additionally, the 3D PCM is used as an electron conduction medium in our VB_{12}-BSA/PCM biosensor, whose increased surface-to-volume ratio greatly prompts the transfer of electrons generated by redox on the ion-selective membrane, ensuring the sensitivity and short response time of the biosensor.

The VB_{12}-BSA/PCM electrode exhibits outstanding performance with a wide linear range of 0.025−45 mM, high sensitivity of 64.08 $\mu A/(mM \cdot cm^2)$ and low LOD of 1 nM, which straddles the levels of salivary nitrite of healthy people (0.06−0.085 mM) and those with nitrite metabolism disorders (0.15−0.2 mM). Moreover, the VB_{12}-BSA/PCM biosensor is ready for mass production for its easy fabrication based on one-step drop casting procedures and negligible variation between batches with a RSD of only 1.29%. Additionally, this biosensor shows high stability with peak current retaining 98% of the original values after 21 days' storage and exhibits good antijamming capability in common drinks and extreme fluid conditions, suggesting that the biosensor with a long working life can meet the demand of practical applications in POC salivary nitrite detection without complex sample pretreatment. Finally, both the VB_{12} bionic enzyme and conductive porous BSA skeleton can be expanded to other applications. For one thing, the VB_{12} bionic enzyme can be regarded as a biocompatible nonmetallic chelating agent immobilized on other electrodes for accurate nitrite detection or nitrite impurity removal. For another, the 3D PCM electrode, which can achieve sensitive and accurate detection of different types of metabolites by coating specific ion-selective layers or immobilizing enzymes, holds potential utility in the diagnosis of a variety of metabolic disorders.

In conclusion, we have proposed a kind of ion-selective amperometric biosensor, which can utilize a bionic enzyme-modified ion-selective membrane to specifically capture target molecules and generate current through a redox reaction, and achieve high electron conduction efficiency with the help of conductive nanomaterials. Based on the concept of this biosensor, we successfully developed a bionic enzyme-assisted ion-selective amperometric biosensor for rapid and sensitive salivary nitrite detection, which is in line with the emerging clinical need of POC nitrite monitoring. The construction and application of this biosensor not only facilitate improved diagnosis, treatment and prognosis of a variety of diseases especially stomach cancer, but also empower long-term health management and dietary conditioning, promoting the realization of precision medicine and smart medicine. We believe the proposed ion-selective amperometric biosensor can be widely adopted in rapid, sensitive, and specific non-enzymatic detection of various ions and biomolecules in the future.

METHODS/EXPERIMENTAL

Materials Preparation. Cyanocobalamin (VB_{12}), carboxyl functionalized gold nanoparticles (AuNPs, diameter 20 nm, ≥ 99%), and artificial saliva (ISO/TR10271) were purchased from Macklin (Shanghai, China). 1-(3-Dimethylaminopropyl)-3-ethylcarbodiimide hydro (EDC) and *N*-hydroxysuccinimide (NHS) were purchased from Sigma (Steinheim, Germany). Potassium ferricyanide ($K_3[Fe(CN)_6]$), potassium hexacyanoferrate(II) ($K_4Fe(CN)_6$), and potassium chloride (KCl) were purchased from Aladdin (Shanghai, China). Multiwalled carbon nanotubes (MWCNTs, diameter 2−5 nm, length 10−30 μm, ≥99%) were purchased from XFNANO (Nanjing, China). Bovine serum albumin (BSA) and sodium nitrite ($NaNO_2$) were purchased from Sigma (Steinheim, Germany). Phosphate buffer solution (PBS, pH = 7.2−7.4) was from Solarbio (Beijing, China). All other chemicals used were of analytical grade without further purification. Double distilled water was used throughout the experiments. All electrochemical measurements were performed on the CHI660E electrochemical workstation (Chenhua, Shanghai, China).

Electrochemical Detection Mechanism of the VB_{12}/BSA-PCM Electrode. The developed 3D VB_{12}/BSA-PCM electrochemical biosensor is based on the three-electrode scheme. First, the VB_{12}-based ion-selective layer identifies and captures the nitrite in complex biological samples with the aid of a strong interaction between trivalent cobalt ions (Co^{3+}) and nitrite. Then, nitrite is oxidized by high-valence Co^{3+}. The electrons lost by nitrite are transferred to PCM-based solid contact layer and the corresponding current can be detected by the electrochemical workstation. The following chemical eqs 2−6 show the detailed detection mechanism of nitrite on a VB_{12}/BSA-PCM electrode.

$$(Co^0Co^{3+})(VB_{12}) + O_2 \rightarrow (Co^{3+})(VB_{12}) + H_2O + 3e^- \quad (2)$$

$$Co^{3+}(VB_{12}) + NO_2^- \leftrightarrow Co^{3+}(NO_2^-)(VB_{12}) \leftrightarrow Co^{2+}(VB_{12}) + NO_2 \quad (3)$$

$$2NO_2 + H_2O \leftrightarrow 2H^+ + NO_3^- + NO_2^- \quad (4)$$

$$NO_2^- + H_2O \rightarrow 2H^+ + NO_3^- + 2e^- \quad (5)$$

$$Co^{2+} \rightarrow Co^{3+}(VB_{12}) + e^- \quad (6)$$

Fabrication of the VB_{12}/BSA-PCM Electrode. The VB_{12}/BSA-PCM electrode was modified by drop casting AuNPs/BSA/CNTs

https://doi.org/10.1021/acsnano.2c05752
ACS Nano 2022, 16, 14849−14859

solution and VB_{12}−AuNPs solution, as shown in Figure 1. First, AuNPs/MWCNTs solution was prepared by adding 5 μL of carboxyl-functionalized AuNPs into 1 mL of MWCNTs solution (0.1 wt %) with ultrasonic mixing for 30 min to achieve complete dispersion. Next, 5 mg of BSA was added to 1 mL of AuNPs/MWCNTs solution. The solution was thoroughly mixed and dispersed by vortex oscillation and ultrasonication until no agglomerates were observed to obtain AuNPs/BSA/CNTs solution. Then, the AuNPs/BSA/CNTs solution was stored in a refrigerator at 4 °C overnight to facilitate the cross-linking between BSA and CNTs. A drop of AuNPs/BSA/CNTs solution (8 μL) was introduced onto the working electrode of screen-printed carbon electrode (SPCE), which was incubated at 55 °C for 2 h to form BSA-PCM.

Afterward, VB_{12} bionic enzyme was immobilized on the surface of BSA-PCM by applying 1 μL of VB_{12}−AuNPs solution (0.3 wt %) and drying at 37 °C for 30 min, and the VB_{12}−AuNPs/BSA/CNTs electrode was thus prepared. The covalent binding between VB_{12} and carboxyl-functionalized AuNPs was formed with the help of EDC/NHS (0.25% EDC/0.09% NHS) after incubating at 37 °C. The working electrode was gently rinsed 3 times with PBS by pipetting, and then the modified biosensor was stored in refrigerator at 4 °C until use.

Topographic Characterization of VB_{12}/BSA-PCM Electrode. Scanning electron microscopy (SEM) studies of bare SPCE working electrode and VB_{12}/BSA-PCM electrode were carried out to confirm the structure of PCM, as shown in Figure 2 and Figure S1. The electrodes were cut into small pieces and placed on a copper disc. Gold particles were deposited on the surface using a spray machine, and electron micrographs were recorded. Energy dispersive spectroscopy (EDS) studies were then carried out to characterize the immobilization of VB_{12}. The morphological study of the biosensor after testing, 3 months storage, and testing following 3 months storage were conducted following the same processes. The thickness of the SPCE before and after modification was tested by an atomic profiler (P-7, KLA-Tencor, China). Transmission electron microscope (TEM) study was conducted by drying the solution of carboxyl modified AuNPs on an ultrathin carbon film.

Electrochemical Characterization of the VB_{12}/BSA-PCM Electrode. The electrochemical performance of the VB_{12}/BSA-PCM electrode was evaluated by a CHI660E electrochemical workstation. First, control experiments between bare SPEC electrode, CNTs-SPEC electrode, BSA-PCM electrode, and VB_{12}/BSA-PCM electrode in 2 mL of $NaNO_2$ solution (5 mM) were performed, and the cyclic voltammetry response was recorded respectively. The potential range during the cyclic voltammetry tests was between 0.6 and 1.6 V, and the scanning rate was set to 100 mV/s. Second, electrochemical impedance spectroscopy (EIS) of SPCE electrode, BSA-PCM electrode, and VB_{12}/BSA-PCM electrode in 1 mM $Fe(CN)_6^{3-/4-}$ (1:1) solution containing 0.1 M KCl were tested, and the Nyquist spectrograms were recorded in order. The equivalent circuit modeling and data fitting were both completed by Zview 3.1 (Scribner Associates, Inc., North Carolina, USA).

Third, to further study the reaction kinetics on the developed VB_{12}/BSA-PCM biosensor, cyclic voltammograms were recorded at different scanning rates, ranging from 20 to 300 mV/s with a 20 mV/s interval. All tests were performed at room temperature (25 °C), and each experiment was repeated three times. After each test, the working electrode was cleaned three times with deionized water (DI water). All cyclic voltammetry data were processed using OriginPro 8.5 (OriginLab Corporation, Northampton, MA).

Optimization of Experimental Condition. To obtain better catalytic performance and optimal signal, the effect of the working potentials to the VB_{12}/BSA-PCM electrode was investigated through amperometric i−t measurement. First, the i−t test was carried out by increasing working potentials in high concentration nitrite solutions from 0.4 to 1.2 V with a 0.2 V intervals. To be specific, the VB_{12}/BSA-PCM electrode was immersed in 2 mL of PBS (0.01 M, pH = 7.4) to obtain the aclinic baseline. Then, 5 μL of $NaNO_2$ (1 M) solution was added every 100 s for five times, ensuring the stability of the double electric layer on the interface and uniform dispersion of the nitrite. After five consecutive drops were added, the current response of each time was averaged. To investigate the optimal potential in low concentration nitrite solution, we followed the same procedures as mentioned above, except the potential range was set to 0.7 to 1.1 V with a 0.1 V interval, and the concentration of added $NaNO_2$ was 10 mM. All tests were performed at room temperature, and each experiment was repeated three times. All the amperometric measurements were conducted in cathodic direction, and the corresponding currents used for data processing were given in absolute values.

Linear Range Measurement of VB_{12}/BSA-PCM Electrode. The linear range and limit of detection (LOD) of the VB_{12}/BSA-PCM electrode were evaluated by recording the i−t response in different concentrations of nitrite. $NaNO_2$ was spiked in PBS (0.01 M, pH = 7.4) to prepare solutions with concentrations varying between 0.025 and 80 mM. Then, the VB_{12}/BSA-PCM biosensor was immersed in 2 mL $NaNO_2$ solutions and amperometric i−t tests were carried out at the optimal working potential. All tests were performed at room temperature and each experiment was repeated three times.

Selectivity, Repeatability, and Stability Assessment of VB_{12}/BSA-PCM Electrode. First, to study the selectivity of the developed VB_{12}/BSA-PCM electrode, an amperometric i−t measurement of the biosensor was carried out by adding five different interferents such as NaCl at 40 mM, $NaHCO_3$ at 25 mM, Na_2CO_3, $NaNO_3$, and Na_2SO_3 at 2 mM, respectively, into 2 mL of 1 mM $NaNO_2$ solution. The interferents chosen were common in human saliva, and their concentration in tests were the highest concentration level in healthy human saliva.

Second, to investigate the repeatability of VB_{12}/BSA-PCM electrode, six electrodes were selected randomly and their i−t response were obtained separately after adding 5 μL of $NaNO_2$ (1 M) in PBS. Afterward, 6 electrodes were soaked in 2 mL of Sprite, milk, ketchup, brine, 12% ethanol, and 37.5% acetic acid solution for 1 h, respectively. Then, the antijamming ability of VB_{12}/BSA-PCM electrode was evaluated in the same i−t measurement of the biosensor at five different measurements at the same test conditions.

Besides, to assess the robustness of the VB_{12}/BSA-PCM electrode, three electrodes were selected randomly and soaked in 2 mL of PBS solution under different pH. Then, 10 μL of $NaNO_2$ (1 M) was added every 200 s for three times to obtain the i−t measurement of the biosensor at five different measurements at the same test conditions. The current response of the three electrodes under different pH was plotted by normalizing the baseline.

Next, to evaluate the stability of the VB_{12}/BSA-PCM electrode, after testing with nitrite solutions at 50, 100, 200, 300 μM and 2, 4, 6, 8, 10 mM, the biosensor was washed by DI water, dried, and stored at room temperature for 21 days. The biosensor was retrieved every 5 days and the performance was investigated by amperometric i−t measurement of the biosensor at five different measurements at the same test conditions. The working potential was set at optimal potential (1.0 V). Each experiment was conducted at room temperature and repeated three times.

Finally, to assess the performance of the VB_{12}/BSA-PCM electrode after durability experiment, the CV measurement of the biosensor storing for 3 months in a 4 °C refrigerator was tested in 2 mL of nitrite solution (5 mM). The potential range during cyclic voltammetry tests was between 0.6 and 1.6 V, and the scanning rate was set to 100 mV/s. Then, the selectivity test was tested following the same procedure mentioned above.

Analysis of Simulated Samples and Real Samples. To investigate the feasibility of the developed VB_{12}/BSA-PCM biosensor for nitrite detection in biological fluids, artificial saliva spiked with $NaNO_2$ to a final concentrations of 0.2, 0.5, 1, 5, 10, and 20 mM was measured by our biosensor. The current response corresponded to the standard curve to calculate the tested concentration of $NaNO_2$, and then the accuracy of $NaNO_2$ detection was assessed. Each experiment was conducted at room temperature and repeated three times.

To evaluate the practicability of the developed VB_{12}/BSA-PCM biosensor for salivary nitrite detection and assess its possibilities in routine monitoring and health management applications, saliva

https://doi.org/10.1021/acsnano.2c05752
ACS Nano 2022, 16, 14849−14859

samples from different volunteers in multiple activity states were collected and analyzed by both our biosensor and a commercial nitrite analyzer within 2 h. To be specific, saliva samples under each test condition were dropped on VB_{12}/BSA-PCM biosensors after centrifuging at 6000 rpm for 15 min at room temperature and removing obvious impurity particles. Then, a stable $i-t$ response was collected under 1.0 V working potential and converted to nitrite concentration according to the fitting curve of the VB_{12}/BSA-PCM biosensor. Each experiment was conducted at room temperature and repeated more than three times, and each VB_{12}/BSA-PCM biosensor was calibrated by simulated saliva. In the control group, the nitrite level in saliva samples was detected by a *p*-aminobenzenesulfonamide kit (Boxbio, Beijing, China). The salivary samples were collected in 2 mL centrifuge tubes and used within 2 h after collection. The six samples used to evaluate the abnormal nitrite detection capability of VB_{12}−PCM biosensor corresponded to volunteers 1−6, respectively. Dynamic measurement of salivary nitrite levels from real samples under different daily activities including sleeping, having lunch, working, and exercising was performed in the same manner, and all the samples were collected from volunteer 2. Experiments involving human saliva samples were performed according to protocols and guidelines approved Ethics Review Committee of Tsinghua University (Beijing, China) and written consent was obtained from all participants.

ASSOCIATED CONTENT

Supporting Information

The Supporting Information is available free of charge at https://pubs.acs.org/doi/10.1021/acsnano.2c05752.

Supporting Figure S1−S6, Table S1: Topographic characterization, condition optimization, repeatability and antijamming ability evaluation, stability assessment, accuracy evaluation (PDF)

AUTHOR INFORMATION

Corresponding Author

Han Wang − *Department of Biomedical Engineering, School of Medicine, Tsinghua University, Beijing 100084, China;* orcid.org/0000-0002-5925-9629; Email: hanwang@tsinghua.edu.cn

Authors

Xueqi Wang − *Department of Biomedical Engineering, School of Medicine, Tsinghua University, Beijing 100084, China*

Jing Cheng − *Department of Biomedical Engineering, School of Medicine, Tsinghua University, Beijing 100084, China; National Engineering Research Center for Beijing Biochip Technology, Beijing 102206, China*

Complete contact information is available at: https://pubs.acs.org/10.1021/acsnano.2c05752

Author Contributions

#H.W. and X.W. contributed equally to this work.

Notes

The authors declare no competing financial interest.

ACKNOWLEDGMENTS

This work was supported by the Spring Breeze Foundation of Tsinghua University to H.W. (20211080032).

REFERENCES

(1) Ferlay, J.; Colombet, M.; Soerjomataram, I.; Parkin, D. M.; Piñeros, M.; Znaor, A.; Bray, F. Cancer statistics for the year 2020: An overview. *Int. J. Cancer.* **2021**, *149*, 778−789.

(2) Buller, I. D.; Patel, D. M.; Weyer, P. J.; Prizment, A.; Jones, R. R.; Ward, M. H. Ingestion of Nitrate and Nitrite and Risk of Stomach and Other Digestive System Cancers in the Iowa Women's Health Study. *Int. J. Environ. Res. Public Health* **2021**, *18*, 6822.

(3) Murray, L. *Goldfrank's Toxicologic Emergencies*, 7th ed.; McGraw-Hill: New York, 2002.

(4) Flores, M.; Toldrá, F. Chemistry, safety, and regulatory considerations in the use of nitrite and nitrate from natural origin in meat products-Invited review. *Meat Sci.* **2021**, *171*, 108272.

(5) Cordero-Herrera, I.; Kozyra, M.; Zhuge, Z.; McCann Haworth, S.; Moretti, C.; Peleli, M.; Caldeira-Dias, M.; Jahandideh, A.; Huirong, H.; Cruz, J. C.; Kleschyov, A. L.; Montenegro, M. F.; Ingelman-Sundberg, M.; Weitzberg, E.; Lundberg, J. O.; Carlstrom, M. AMP-activated protein kinase activation and NADPH oxidase inhibition by inorganic nitrate and nitrite prevent liver steatosis. *Proc. Natl. Acad. Sci. U. S. A.* **2019**, *116*, 217−226.

(6) Velmurugan, S.; Gan, J. M.; Rathod, K. S.; Khambata, R. S.; Ghosh, S. M.; Hartley, A.; Van Eijl, S.; Sagi-Kiss, V.; Chowdhury, T. A.; Curtis, M.; Kuhnle, G. G.; Wade, W. G.; Ahluwalia, A. Dietary nitrate improves vascular function in patients with hypercholesterolemia: a randomized, double-blind, placebo-controlled study. *Am. J. Clin. Nutr.* **2016**, *103*, 25−38.

(7) Ma, L.; Hu, L.; Feng, X.; Wang, S. Nitrate and Nitrite in Health and Disease. *Aging and Disease* **2018**, *9*, 938−945.

(8) El Hani, O.; Karrat, A.; Digua, K.; Amine, A. Development of a simplified spectrophotometric method for nitrite determination in water samples. *Spectrochim Acta A Mol. Biomol Spectrosc* **2022**, *267*, 120574.

(9) Han, S.; Chen, X. Copper nanoclusters-enhanced chemiluminescence for folic acid and nitrite detection. *Spectrochim Acta A Mol. Biomol Spectrosc* **2019**, *210*, 315−320.

(10) Wang, Q. H.; Yu, L. J.; Liu, Y.; Lin, L.; Lu, R. G.; Zhu, J. P.; He, L.; Lu, Z. L. Methods for the detection and determination of nitrite and nitrate: A review. *Talanta* **2017**, *165*, 709−720.

(11) Yan, H.; Zhuo, X.; Shen, B.; Xiang, P.; Shen, M. Determination of Nitrite in Whole Blood by High-Performance Liquid Chromatography with Electrochemical Detection and a Case of Nitrite Poisoning. *J. Forensic Sci.* **2016**, *61*, 254−258.

(12) Hassan, M.; Abbas, G.; Li, N.; Afzal, A.; Haider, Z.; Ahmed, S.; Xu, X.; Pan, C.; Peng, Z. Significance of Flexible Substrates for Wearable and Implantable Devices: Recent Advances and Perspectives. *Adv. Mater. Technol.* **2022**, *7*, 2100773.

(13) Zhang, S.; Tang, Y.; Chen, Y.; Zheng, J. Synthesis of gold nanoparticles coated on flower-like MoS2 microsphere and their application for electrochemical nitrite sensing. *J. Electroanal. Chem.* **2019**, *839*, 195−201.

(14) Chen, G.; Zheng, J. Non-enzymatic electrochemical sensor for nitrite based on a graphene oxide-polyaniline-Au nanoparticles nanocomposite. *Microchem. J.* **2021**, *164*, 106034.

(15) Duan, C.; Bai, W.; Zheng, J. Non-enzymatic sensors based on a glassy carbon electrode modified with Au nanoparticles/polyaniline/SnO_2 fibrous nanocomposites for nitrite sensing. *New J. Chem.* **2018**, *42*, 11516−11524.

(16) Néel, B.; Ghahraman Asfhar, M.; Crespo, G. A.; Pawlak, M.; Dorokhin, D.; Bakker, E. Nitrite-Selective Electrode Based On Cobalt(II) tert-Butyl-Salophen Ionophore. *Electroanalysis* **2014**, *26*, 473−480.

(17) Wang, J.; Zhan, G.; Yang, X.; Zheng, D.; Li, X.; Zhang, L.; Huang, T.; Wang, X. Rapid detection of nitrite based on nitrite-oxidizing bacteria biosensor and its application in surface water monitoring. *Biosens Bioelectron* **2022**, *215*, 114573.

(18) Yilmaz, H.; Kocak, A.; Dilimulati, M.; Zorlu, Z.; Andac, M. A new Co(III) complex of Schiff base derivative for electrochemical recognition of nitrite anion. *J. Chem. Sci.* **2017**, *129*, 1559−1569.

(19) Sabaté Del Río, J.; Henry, O.; Jolly, P.; Ingber, D. E. An antifouling coating that enables affinity-based electrochemical biosensing in complex biological fluids. *Nat. Nanotechnol.* **2019**, *14*, 1143−1149.

(20) Li, Y.; Han, R.; Chen, M.; Zhang, L.; Wang, G.; Luo, X. Bovine serum albumin-cross-linked polyaniline nanowires for ultralow fouling and highly sensitive electrochemical protein quantification in human serum samples. *Anal. Chem.* **2021**, *93*, 4326−4333.
(21) Strong, M. E.; Richards, J. R.; Torres, M.; Beck, C. M.; La Belle, J. T. Faradaic electrochemical impedance spectroscopy for enhanced analyte detection in diagnostics. *Biosens Bioelectron* **2021**, *177*, 112949.
(22) Lin, S. L.; Hsu, J. W.; Fuh, M. R. Simultaneous determination of nitrate and nitrite in vegetables by poly(vinylimidazole-co-ethylene dimethacrylate) monolithic capillary liquid chromatography with UV detection. *Talanta* **2019**, *205*, 120082.
(23) Xu, Z.; Shi, W.; Yang, C.; Xu, J.; Liu, H.; Xu, J.; Zhu, B. A colorimetric fluorescent probe for rapid and specific detection of nitrite. *Luminescence* **2020**, *35*, 299−304.
(24) Wu, H.; Shen, X.; Huo, D.; Ma, Y.; Bian, M.; Shen, C.; Hou, C. Fluorescent and colorimetric dual-readout sensor based on Griess assay for nitrite detection. *Spectrochim Acta A Mol. Biomol Spectrosc* **2020**, *225*, 117470.
(25) Saeb, E.; Asadpour-Zeynali, K. A novel ZIF-8@ZIF-67/Au core−shell metal organic framework nanocomposite as a highly sensitive electrochemical sensor for nitrite determination. *Electrochim. Acta* **2022**, *417*, 140278.
(26) Pan, F.; Chen, D.; Zhuang, X.; Wu, X.; Luan, F.; Zhang, S.; Wei, J.; Xia, S.; Li, X. Fabrication of gold nanoparticles/l-cysteine functionalized graphene oxide nanocomposites and application for nitrite detection. *J. Alloys Compd.* **2018**, *744*, 51−56.
(27) Sudha, V.; Kumar, S. M., III; Thangamuthu, R. Simultaneous electrochemical sensing of sulphite and nitrite on acid-functionalized multi-walled carbon nanotubes modified electrodes. *J. Alloys Compd.* **2018**, *749*, 990−999.
(28) Jiang, J.; Fan, W.; Du, X. Nitrite electrochemical biosensing based on coupled graphene and gold nanoparticles. *Biosens Bioelectron* **2014**, *51*, 343−348.
(29) Raja Jamaluddin, R.; Yook Heng, L.; Tan, L. L.; Chong, K. F. Electrochemical Biosensor for Nitrite Based on Polyacrylic-Graphene Composite Film with Covalently Immobilized Hemoglobin. *Sensors (Basel).* **2018**, *18*, 1343.
(30) Ndala, A.; Itota, B.; Chamier, J.; Ray, S.; Sunday, C.; Chowdhury, M. Novel ($CH_6N_3^+$, NH_3^+)-functionalized and nitrogen doped Co_3O_4 thin film electrochemical sensor for nanomolar detection of nitrite in neutral pH. *Electrochim. Acta* **2021**, *388*, 138556.
(31) Meschiari, C. A.; Zuardi, L. R.; Gomes, V. A.; Costa de Almeida, G. R.; Novaes, A. B., Jr; Gerlach, R. F.; Marcaccini, A. M. Salivary, blood and plasma nitrite concentrations in periodontal patients and healthy individuals before and after periodontal treatment. *Clin. Chim. Acta* **2015**, *444*, 293−296.

https://doi.org/10.1021/acsnano.2c05752
ACS Nano 2022, 16, 14849−14859